GEOLOGY | THE GEOLOGICAL SOCIETY OF AMERICA®

https://doi.org/10.1130/G50689.1

Manuscript received 22 August 2022
Revised manuscript received 18 November 2022
Manuscript accepted 3 December 2022

Published online 23 February 2023

Dolomite cement microstratigraphy: A record of brine evolution and ore precipitation mechanisms, upper Knox Group, Tennessee and Kentucky, USA

J. Richard Kyle[1,2], Thomas R. Quintero[1], Estibalitz Ukar[2], Nathan R. Miller[1], Sara J. Elliott[2] and Matthew Colbert[1]
[1]Department of Geological Sciences, Jackson School of Geosciences, University of Texas at Austin, Austin, Texas 78712, USA
[2]Bureau of Economic Geology, Jackson School of Geosciences, University of Texas at Austin, Austin, Texas 78713, USA

ABSTRACT

Trace element changes in fluids associated with ore-forming events in sedimentary basins may be recorded by contemporaneous cements, especially zoned carbonate minerals (microstratigraphy). Cement analysis using advanced mapping and analytical techniques including scanning electron microscopy cathodoluminescence (SEM-CL), charge contrast imaging, high-resolution X-ray computed tomography (XCT), and laser ablation–inductively coupled plasma–mass spectrometry (LA-ICP-MS) documents geochemical changes associated with Mississippi Valley–type mineralization in solution-collapse breccias of the Cambrian–Ordovician Knox Group (Tennessee and Kentucky, USA). Dolomite cement zonation coincident with changes in Fe and Mn can be observed with optical microscope CL in bands as narrow as 5 µm, whereas panchromatic SEM-CL reveals microfractures and cement subzones coincident with changes in La and Ce concentrations in bands as narrow as 0.1 µm. XCT scans image a high-density (Fe-rich) dolomite zone at the onset of late sulfide precipitation. The transition from pre-ore to ore-stage cementation is marked by increased Fe, Mn, Zn, Cd, Ga, Pb, and Sr and decreased La and Ce concentrations. Fine-scale metal depletion cycles during this transition may record metal precipitation from brine in response to the availability of reduced sulfur. Except for Fe and Mn, post-ore dolomite zones generally have low metal concentrations. Thus, dolomite microstratigraphy tracks systematic changes in brine metal concentrations modified by episodes of localized sulfide mineral precipitation.

INTRODUCTION

Geochemical episodes associated with ore-forming events and creation and/or occlusion of secondary porosity in carbonate strata are of great importance for understanding mineral resources and their associations with groundwater, brines, and hydrocarbons. Cambrian–Ordovician strata of the Great American Carbonate Bank (Knox Group [southeastern United States] and equivalents) provide exceptional examples of these relationships (Fig. 1). These strata contain widespread solution-collapse breccia systems that are cemented by carbonate minerals and locally host commercial concentrations of important resources, including Mississippi Valley–type (MVT) ores (Leach et al., 2010; Gregg and Shelton, 2012).

Ore minerals and fluid inclusions within them offer a partial record of chemical conditions during mineralization. Microstratigraphic studies of associated carbonate cements can further elucidate mechanisms of ore formation, including pre-mineralization conditions, because chemical fluctuations in mineralizing fluids are recorded as growth zones with spatial variations in elemental composition (Reeder, 1991).

Many studies have investigated Knox Group breccia bodies in the Tennessee region, including the use of optical microscope cathodoluminescence (OM-CL) to define dolomite cement microstratigraphy and attempted correlation over large areas (Ebers and Kopp, 1979; Kopp et al., 1986; Stefani, 1995; Montañez, 1996, 1997). Studies have focused on OM-CL zoning caused by variations in Ca, Mg, Sr, Fe, and Mn, of which Fe and Mn contents are of critical importance (Fairchild, 1983; Hemming et al., 1989; Machel and Burton, 1991; Machel et al., 1991; Richter et al., 2003; Hiatt and Pufahl, 2014). Variations of other metals and rare earth element (REE) concentrations are less understood, albeit more important because of their association with mineralization.

Advances in laser ablation–inductively coupled plasma–mass spectrometry (LA-ICP-MS) enable near-simultaneous elemental analysis at scales of <10 µm, allowing for fine-scale microchemical characterization of carbonate microstratigraphic zones (Sylvester and Jackson, 2016). Similarly, advances in high-resolution scanning electron microscopy cathodoluminescence (SEM-CL) and charge contrast imaging (CCI), can reveal submicron-scale trace element variations in carbonates (Ukar and Laubach, 2016). Innovations in high-resolution X-ray computed tomography (XCT) permit quantitative assessments of cement inclusions and their three-dimensional distributions, particularly of metallic minerals (Kyle and Ketcham, 2015). These recent analytical advancements encourage revisiting carbonate cement microstratigraphy as a record of mineralization events.

We used multiple imaging techniques to evaluate elemental changes in zoned dolomite cements in carbonate breccias that locally contain MVT ore minerals. We found that dolomite microstratigraphy follows systematic geochemical variations in metal and REE concentrations that correspond to episodes of sulfide mineral precipitation. The results of this study can be applied to carbonate breccia systems that are widespread globally to better assess genetic controls for critical mineral concentrations.

BACKGROUND GEOLOGY

The 1-km-thick Knox Group is a widespread outcrop and/or subcrop component of the Cambrian–Ordovician "Great American Carbonate Bank" (Fig. 1A; Gregg and Shelton, 2012). Upper Knox Group carbonates comprise a sequence of shallowing-upward, 0.5–13-m-thick peritidal cycles (Montañez and Read, 1992). Groundwater circulation during post–Early Ordovician regional exposure led to widespread dissolution

CITATION: Kyle, J.R., et al., 2023, Dolomite cement microstratigraphy: A record of brine evolution and ore precipitation mechanisms, upper Knox Group, Tennessee and Kentucky, USA: Geology, v. 51, p. 392–396, https://doi.org/10.1130/G50689.1

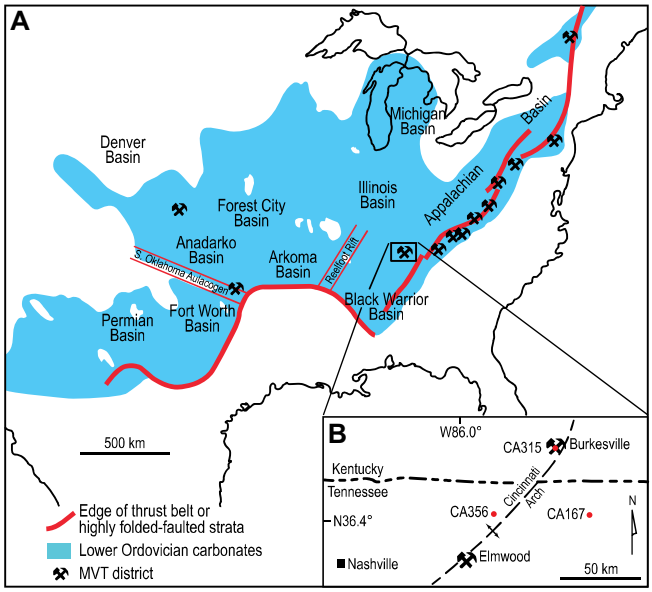

Figure 1. Map of the study area. (A) Lower Ordovician portion of the Great American Carbonate Bank in southern North America, showing major Mississippi Valley–type (MVT) zinc districts. Modified from Gregg and Shelton (2012). (B) Study area in central Tennessee and southern Kentucky showing mines and core locations. Middle Ordovician through Mississippian strata overlie Knox Group carbonates in the study area.

and subsequent collapse brecciation of carbonate strata (Hoagland, 1976). Breccia systems are broadly similar over a > 50,000 km^2 area, with cementation dominated by coarse hydrothermal carbonates (e.g., saddle dolomite, calcite) and local MVT mineralization (sphalerite, galena, fluorite, barite) in eastern and central Tennessee (Kyle, 1976; Gaylord and Briskey, 1983; Montañez, 1997; Fig. 1). Fluid inclusion studies indicate that ore minerals precipitated from high-salinity brines (21–23 wt% NaCl equivalent) at 100–130 °C (Gratz and Misra, 1987; Stefani, 1995). Initial exploration models for central Tennessee assumed that mineralization was due to basinal brines derived from the Alleghanian tectonic system, as had been proposed for eastern Tennessee ores (Crawford and Hoagland, 1968; Hoagland, 1976; Fig. 1). However, subsequent studies have documented notable differences among districts (e.g., Kyle, 1976; Lewchuk and

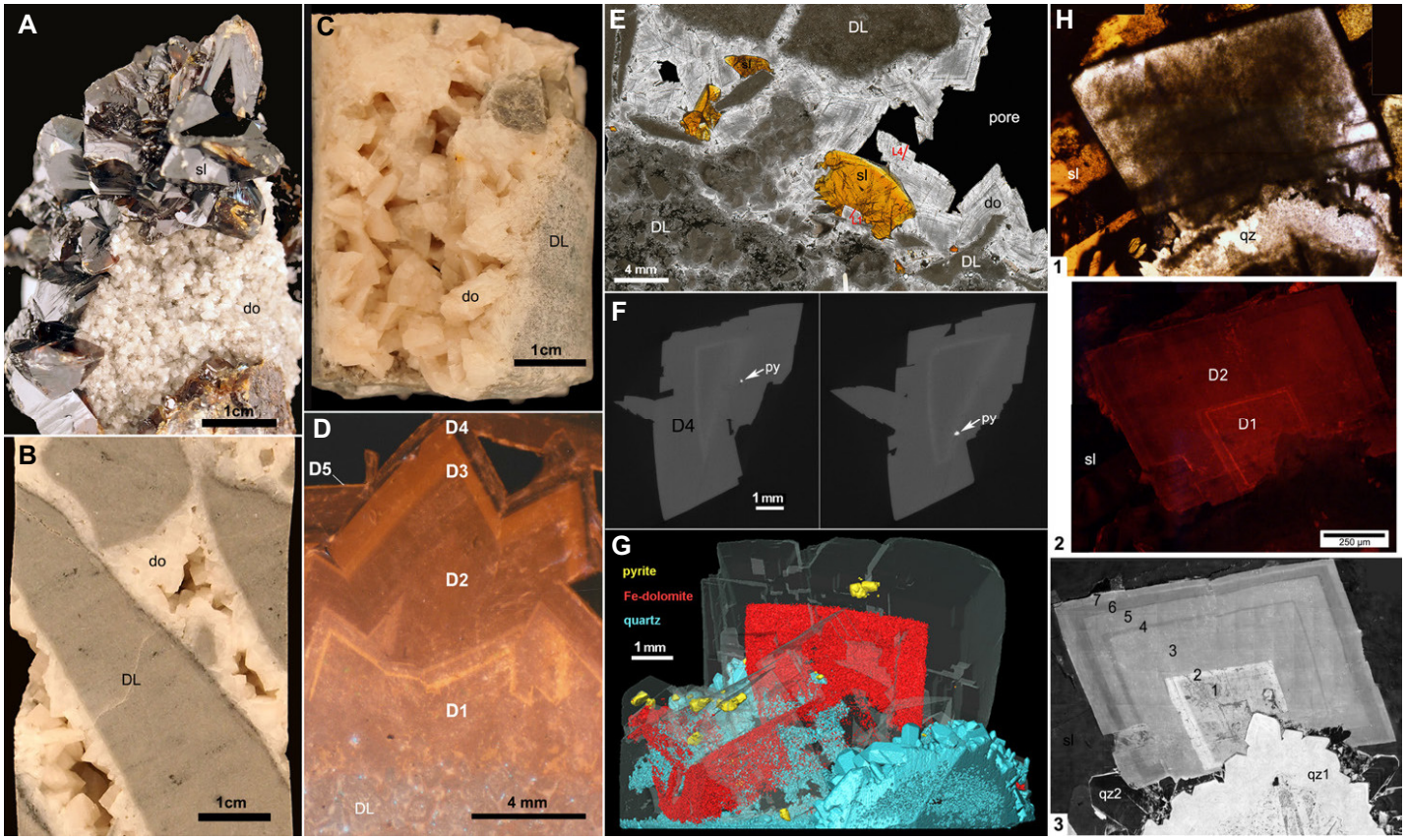

Figure 2. Examples of pre-, syn-, and post-ore dolomite cement and sulfide minerals. (A) Early dolomite breccia cement overgrown by coarse sphalerite, Elmwood mine in the Knox Group, Tennessee, USA. (B) Sawed core of breccia cemented by coarse saddle dolomite (sample CA356-1888). (C) Core with pink dolomite cement (CA167-2482). (D) Optical microscope cathodoluminescence (OM-CL) of dolomite cement showing mineralization zones D1–D5 (CA356-1888). (E) Thick polished section of mineralized breccia cemented by pre-ore dolomite, sphalerite, and post-ore dolomite with select laser ablation tracks (red lines) (CA315-2305). (F) Grayscale X-ray computed tomography (XCT) slices showing lighter ferroan dolomite zone (interior D4) with associated ~100 µm pyrite inclusions (shown by arrows) (CA167-2483). (G) XCT model of dolomite cement on quartz cement of breccia, with the younger dolomite cement rendered transparent to show ferroan dolomite zone (interior D4) with associated coarse pyrite (CA167-2483); see the Supplemental Material (see footnote 1) for animation. (H) Comparison of petrographic and imaging techniques for early dolomite crystal on quartz and overgrown by sphalerite in thick polished section (KY2-30). 1—Plane-polarized image showing the turbid core of the dolomite crystal and a less-turbid rim overgrown by sphalerite. 2—OM-CL image of D1 and D2 dolomite zones. 3—scanning electron microscopy cathodoluminescence (SEM-CL) image showing fine zonation in the dolomite crystal and microfractures that terminate within D1. Two generations of pre-dolomite quartz cement are present. DL—dolostone; do—dolomite; py—pyrite; qz—quartz; sl—sphalerite.

Symons, 1996; Potra and Moyers, 2017), suggesting more complex regional systems.

Our study investigates coarse dolomite crystals in upper Knox Group breccias from mines and three core locations spanning ~1000 km² in central Tennessee and southern Kentucky (Fig. 1B). We analyzed petrographic sections, selected to evaluate dolomite cement bracketing and coincident with sulfide mineralization, using a combination of transmitted-light petrography, OM-CL, SEM-CL imaging and spectrometry, CCI using a variable-pressure secondary electron detector, XCT, and LA-ICP-MS trace element analysis (see the Supplemental Material[1] for details of the methodology).

RESULTS

We studied pore-filling euhedral dolomite crystals (0.1–10 mm in maximum dimension) precipitated within brecciated dolostone and/or on early quartz cement substrates (Fig. 2). Based on overlapping criteria, we determined that dolomite crystals precipitated prior to sphalerite, during sulfide deposition as indicated by pyrite inclusions within dolomite, and following ore-stage mineralization as evidenced by dolomite crystal growth on sphalerite crystals (Figs. 2A–2E). Dolomite cement stratigraphy in this system thus potentially tracks fluids associated with pre-, syn-, and post-mineralization conditions.

Dolomite Zoning

Most dolomite crystals appear coarsely zoned in plane-polarized light irrespective of their relative age (Figs. 2D and 2E). Dolomites are red under OM-CL with distinct zones of differing CL intensity (Fig. 2D). Most zones evident in OM-CL are >30 μm, and many coincide with those delineated by inclusions (Fig. 2H1). Based on CL intensity and overlapping criteria, we distinguished two pre-ore mineralization zones (D1 and D2) in dolomite crystal cores, a zone (D3) that broadly coincides with the main stage of sphalerite mineralization, and two late zones (D4 and D5) that include local sulfide precipitation as indicated by pyrite inclusions within dolomite crystals (Figs. 2D–2G). Pre- to ore-stage dolomite cements (D1–D3) generally display brighter OM-CL than post-ore cement (D4). D5 is generally thin but appears to correspond with some dolomite crystals that are pink in hand sample (Figs. 2C and 2D). SEM-CL reveals multiple, finer-scale, rhythmic zones within these five general zones and other textures invisible to OM-CL such as anastomosing irregular textures in D1 cores and several generations of cross-cutting microfractures (Fig. 2H). The narrowest zone visible under OM-CL is ~5–10 μm, compared to ~100-nm-wide zones and ≥10-nm-wide microfractures visible in SEM-CL (Fig. 2H3). Thickness of concentric zones varies considerably in petrographic sections due to growth and cut effects.

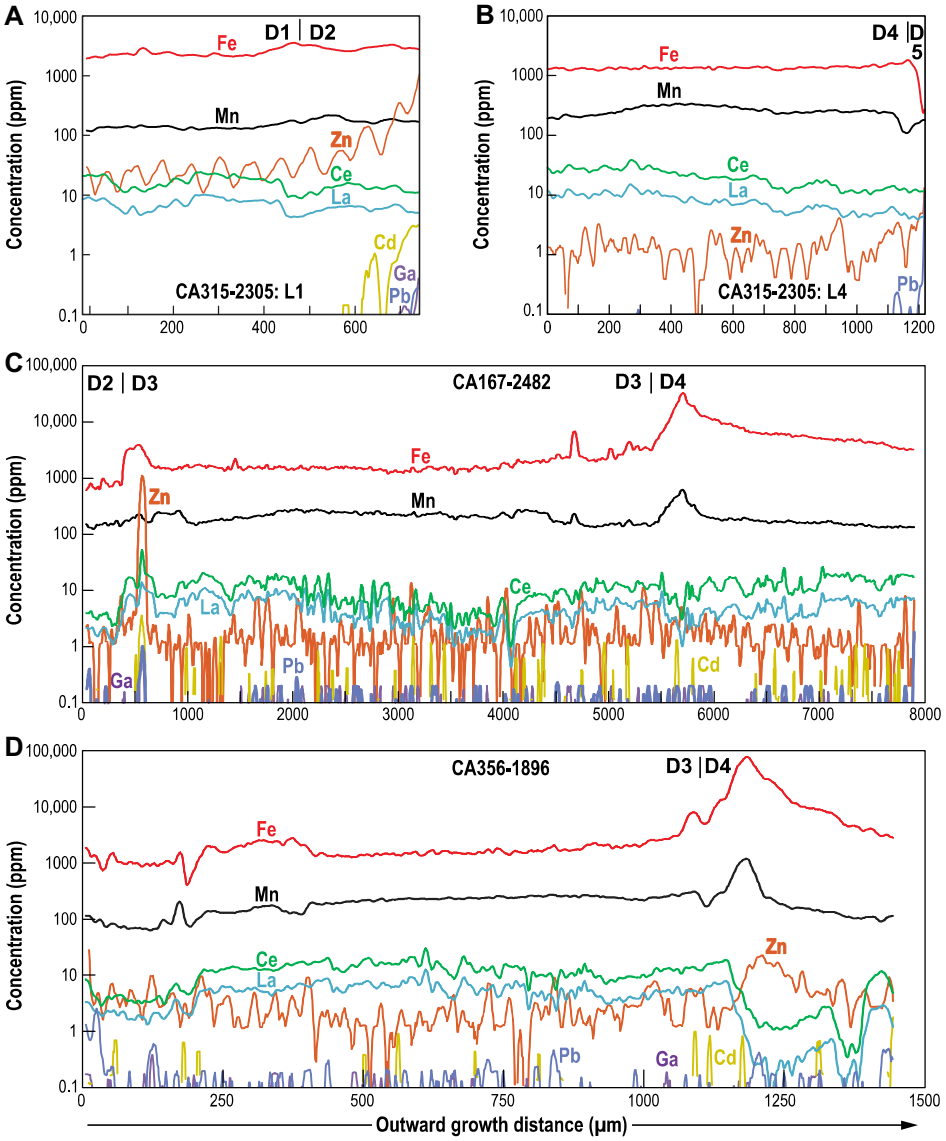

Figure 3. Laser ablation–inductively coupled plasma–mass spectrometry (LA-ICP-MS) analyses (in ppm) along traverses in pre-ore and post-ore dolomite. (A) LA-ICP-MS analysis of the early white dolomite (mineralization zones D1–D2) overgrown by sphalerite along traverse L1 (sample CA315-2305; Fig. 2E). D2 zone has high Zn and spotty Cd, Ga, and Pb concentrations. Note the increase in Zn and associated metals leading up to sphalerite precipitation. (B) LA-ICP-MS analysis of post-sphalerite dolomite (D4–D5) along traverse L4 (sample CA315-2305; Fig. 2E). Note the abrupt Fe decrease at the dolomite crystal perimeter, which corresponds to precipitation of pyrite and a bright optical microscope cathodoluminescence (OM-CL) zone (D5) in the dolomite due to higher relative Mn. (C) LA-ICP-MS analysis of dolomite cement (D2–D4) with late pyrite (CA167-2482; Figs. 2F–2G). (D) LA-ICP-MS analysis of dolomite cement (D3–D4) in unmineralized breccia (CA356-1896; Fig. 2D).

Elemental Variations Related to Dolomite Zoning

LA-ICP-MS transects highlight differences in elemental concentrations among dolomite zones, especially in Fe, Mn, La, and Ce and, in some cases, Zn, Cd, Ga, Pb, Ba, Sr, and Eu (Fig. 3). This elemental suite is typical of MVT systems and specifically for this region (Bonnet et al., 2016). OM-CL zones best correlate with changes in Mn versus Fe with brighter zones having higher Mn/(Mn + Fe). The darkest OM-CL zone (interior D4) has the highest Fe (as much as 8.9 wt%) and lowest Mn/(Mn + Fe), whereas the brightest outermost zones within D1 have the lowest Fe concentrations (Fe ~550 ppm versus 2000 ppm for medium-bright zones) (Table 1; Fig. 2D). The difference in Fe content between the interior

[1]Supplemental Material. Sample descriptions and locations; detailed methodology; and high-resolution X-ray computed tomography animation of sample CA167-2483. Please visit https://doi.org/10.1130/GEOL.S.21992501 to access the supplemental material, and contact editing@geosociety.org with any questions.

TABLE 1. AVERAGE CHEMICAL CONCENTRATION (IN PPM) OF TRACE ELEMENTS IN SELECT SAMPLES BINNED BY OPTICAL CL ZONE

Sample	Zone	Mn/(Mn + Fe)	Mn	Fe	Co	Cu	Zn	Ga	Ge	As	Sr	Y	Cd	^{137}Ba	^{138}Ba	La	Ce	Eu	Pb	U	Ni
KY2-19	D-1	0.09	86	886	0.2	0.2	10.0	0.0	0.3	0.2	60	1.3	0.1	0.6	0.6	2.2	4.1	0.1	0.1	0.1	N.A.
CA167-2482	D-1	0.17	149	768	0.2	0.5	1.5	0.1	0.4	0.5	58	1.0	0.3	0.8	1.5	1.8	3.4	0.1	0.2	0.0	N.A.
CA315-2305 T3	D-1	0.10	119	1220	0.5	1.4	14.7	0.5	1.5	1.4	96	1.3	2.2	3.6	3.9	3.2	7.0	0.1	0.5	0.4	N.A.
KY2-30 A	D-1	0.07	117	1595	0.2	4.1	6.9	0.1	N.A.	1.2	55	0.9	0.2	1.6	1.6	2.0	4.2	0.1	3.1	0.0	N.A.
KY2-30 B1	D-1	0.10	112	1167	0.1	3.3	62.6	0.1	N.A.	0.8	56	0.8	0.6	0.6	0.5	1.8	3.9	0.1	2.6	0.0	N.A.
KY2-30 B2	D-1	0.09	102	1061	0.1	4.2	23.3	0.1	N.A.	0.9	54	0.8	0.5	0.5	0.5	1.6	3.3	0.1	3.2	0.1	N.A.
	D-1 Avg.	0.10	114	1116	0.2	2.3	19.8	0.2	0.4	0.8	63	1.0	0.7	1.3	1.4	2.1	4.3	0.1	1.6	0.1	
CA167-2482	D-2	0.08	182	2444	0.1	0.3	9.9	0.0	0.2	0.1	47	1.1	0.1	0.8	1.0	6.8	13.8	0.2	0.1	0.0	N.A.
CA315-2305 L5	D-2	0.06	197	3242	N.A.	0.2	3.3	0.0	N.A.	0.2	44	1.0	0.1	1.0	0.9	4.0	9.1	0.1	0.1	N.A.	0.3
CA315-2305 T1	D-2	0.07	167	2236	0.3	1.1	2.9	0.2	1.2	1.6	70	2.6	0.9	0.8	0.8	8.7	20.5	0.2	0.1	N.A.	N.A.
KY2-30 A	D-2	0.04	150	3644	0.1	2.0	16.8	0.1	N.A.	1.1	48	2.6	0.8	0.5	0.6	10.1	26.1	0.3	2.0	0.0	N.A.
KY2-30 B1	D-2	0.05	158	3057	0.1	1.2	55.1	0.1	N.A.	0.9	50	2.3	1.2	0.2	0.2	8.4	22.1	0.2	1.6	0.0	N.A.
KY2-30 B2	D-2	0.05	147	2851	0.1	1.9	48.5	0.1	N.A.	1.1	51	1.6	0.4	0.4	0.3	5.7	14.4	0.2	1.8	0.0	N.A.
	D-2 Avg.	0.06	167	2912	0.1	1.1	22.7	0.1		0.8	52	1.9	0.6	0.6	0.6	7.3	17.7	0.2	0.9	0.0	
CA167-2482	D-3	0.11	211	1866	0.1	0.3	2.3	0.1	0.6	0.5	51	1.0	0.4	0.4	0.3	4.9	9.6	0.3	0.2	0.0	N.A.
CA315-2305 L5	D-3	0.10	279	2547	N.A.	0.2	2.7	0.0	N.A.	0.2	53	1.4	0.0	0.9	0.9	4.5	10.3	0.1	0.1	N.A.	0.4
CA315-2305 L6	D-3	0.09	225	2471	N.A.	0.2	2.1	0.0	N.A.	0.1	56	1.2	0.0	0.1	0.2	3.8	8.3	0.1	0.1	N.A.	0.2
CA356-1896	D-3	0.12	238	1948	0.1	0.5	2.6	0.1	0.6	0.5	53	1.7	0.4	0.3	0.3	5.8	13.4	0.2	0.1	0.0	N.A.
	D-3 Avg.	0.11	238	2208	0.1	0.3	2.4	0.1	0.3	0.3	53	1.3	0.2	0.4	0.4	4.8	10.4	0.2	0.1	0.0	0.2
CA167-2482	D-4	0.03	197	7896	0.2	0.3	2.4	0.1	1.0	0.5	54	1.5	0.4	0.5	0.5	5.0	13.7	0.3	0.1	0.0	N.A.
CA315-2305 L5	D-4	0.04	189	7248	N.A.	0.2	3.2	0.1	N.A.	0.5	62	1.0	0.1	1.0	1.1	2.7	7.9	0.1	0.1	N.A.	0.5
CA315-2305 L6	D-4	0.03	207	9105	N.A.	0.1	3.9	0.1	N.A.	0.1	68	1.1	0.1	0.5	0.6	3.0	7.6	0.1	0.0	N.A.	0.4
CA315-2305 T2	D-4	0.05	304	11,196	0.4	0.3	5.4	0.0	0.9	0.3	109	1.0	N.A.	0.6	0.4	2.4	6.6	0.2	0.1	0.0	N.A.
CA356-1896	D-4	0.02	272	17,466	0.2	0.4	7.3	0.1	2.0	0.6	99	1.1	0.5	0.6	0.3	1.8	5.3	0.2	0.2	0.0	N.A.
	D-4 Avg.	0.03	234	10,582	0.2	0.3	4.4	0.1	0.8	0.4	78	1.1	0.2	0.6	0.6	3.0	8.2	0.2	0.1	0.0	0.2
CA315-2305 L5	D-5	0.14	260	1575	N.A.	0.6	37.8	0.1	N.A.	0.2	44	1.7	0.1	0.7	0.7	6.6	18.5	0.3	1.4	N.A.	0.9
CA315-2305 L6	D-5	0.13	248	1605	N.A.	0.1	1.4	2.8	N.A.	0.2	46	1.8	0.1	0.3	0.3	6.9	19.6	0.4	0.1	N.A.	0.3
CA315-2305 T2	D-5	0.15	297	1895	0.3	0.6	2.2	0.0	0.3	N.A.	70	2.1	0.2	0.5	0.3	8.6	24.6	0.4	0.2	0.0	N.A.
	D-5 Avg.	0.14	268	1692		0.4	13.8	1.0		0.1	53	1.9	0.1	0.5	0.4	7.4	20.9	0.4	0.6		0.4

Note: CL—cathodoluminescence; N.A.—not analyzed; Avg.—average (averages are not shown for elements with <50% data).

D4 zone and subsequent zones is so great that the D4 ferroan dolomite can be imaged with XCT, showing Fe-rich cores enveloped by Fe-poor dolomite shells containing pyrite inclusions (Figs. 2F and 2G). Subzones revealed by SEM-CL and CCI, but invisible to OM-CL, correlate with subtle changes in La, Ce, and Fe. For example, the transition between non-luminescent interior D4 to weakly luminescent external D4 corresponds with an increase in Fe and Mn and a decrease in La and Ce, whereas the bright-luminescent outermost zone (D5) correlates with an increase in La and Ce content and a depletion in Fe, yielding a higher Mn/(Mn + Fe) ratio (Fig. 3B; Table 1). Finer-scale luminescent zones revealed by SEM-CL are not well explained by Mn/(Mn + Fe) but may track other trace element enrichments (Ba, Sr, Zn, Cd, La, Ce) in host cement (Quintero, 2020).

Pre- to ore-stage zones (D1 to D3) generally contain higher Mn/(Mn + Fe) than the post-ore cement (D4) (Table 1). Zn shows cyclic increases from a base of 10 ppm to >100 ppm toward the onset of sphalerite precipitation (Fig. 3A). This Zn spike is accompanied by increases in Fe, Mn, Ba, La, and Ce. All samples display striking Fe and Mn increases and La and Ce decreases at the D3-D4 boundary (Table 1). Post-sphalerite dolomite has a Zn content of a few parts per million (Table 1; Figs. 3B–3D).

DISCUSSION

We hypothesize that dolomite cements effectively record pulses of higher-metal-content brines from which MVT minerals precipitated. The brines responsible for ore mineralization were most likely regional because distinct zones can be recognized in samples over an area >1000 km^2 (Fig. 1). Syn-ore zone D3 marks the infiltration of fluids rich in Fe (and other metals) and precipitation of sulfides. The observed increase in MVT metals within D2 suggests a brine with increased metal content (Fig. 3A), leading to precipitation of Zn-rich ores. Late D4 and D5 zones have less La and Ce, perhaps reflecting the nature and composition of the late Fe-rich brines (Table 1). Pyrite inclusions throughout post-ore D4 and D5 zones demonstrate that conditions appropriate for local sulfide precipitation spanned multiple dolomite cement stages. However, the principal Zn precipitation stage at the D2-D3 transition suggests that the regional fluid was stripped of its major MVT metals relatively early in the cement sequence.

Studies of Knox Group breccia bodies have generally concluded that regional brine systems differed in timing (Lewchuk and Symons 1996; Kesler et al., 2004), ore component sources, and precipitation mechanisms (Kesler et al., 1994; Potra and Moyers, 2017). Regional differences in fluid mixing and fluid-rock interaction may also account for fine-scale differences in carbonate cement zonal patterns. Abundant H_2S, likely derived by thermochemical sulfate reduction or other mechanisms, is critical for local sulfide precipitation from regional brines (Kesler et al., 1994; Anderson, 2008). Reaction-path modeling suggests that carbonate precipitation is incompatible with the presence of abundant H_2S at a sphalerite precipitation site (Anderson and Garven, 1987). When H_2S is absent, dolomite precipitation from metal-bearing brines could incorporate anomalous amounts of metals, such as the D4 ferroan dolomite. If limited H_2S is present, minor Fe sulfides could precipitate from Fe-dominant brines. The timing and abundance of H_2S at the depositional site could thus account for the occurrence of rare "ore" sites (e.g., Elmwood, Burkesville) versus extensive "barren" dolomite-cemented breccia systems (e.g., sites CA167 and CA356) (Fig. 1B). However, the ore-stage brine may be represented by local Zn-rich dolomite cement zones, even in breccias lacking appreciable sphalerite concentrations (Fig. 3C). Our study suggests that dolomite microstratigraphy can record systematic changes in fluid metal concentrations operating at regional and local scales that, depending on H_2S abundance, may be accompanied by sulfide mineral precipitation.

CONCLUSIONS

New imaging and analytical techniques applied to MVT dolomite cements enhance understanding of brine compositions before, during, and after ore mineralization that bear on ore mineral precipitation mechanisms. Marked increases in Fe and/or Zn associated with mineralization are commonly accompanied by changes in La and Ce concentrations that appear to correspond with narrow cement zones observed using SEM-CL. Relatively consistent zones observed with OM-CL occur regionally, supporting broad patterns of basinal brine evolution and advection, but local zoning differences indicate that specific precipitation conditions varied among localities. Early brines forming pre-mineralization dolomites contained low concentrations of metals, resulting in zoned dolomites whose MVT metals increased over time. Later metal-bearing brines encountered local concentrations of reduced sulfur that resulted in rare MVT-mineralized zones.

Dolomites that precipitated with, or shortly following, Zn precipitation may be zoned, but nonluminescent Fe-rich bands suggest that reduced sulfur levels were insufficient to cause extensive sulfide precipitation. Local pyrite-bearing zones suggest the presence of reduced sulfur, but the brines lacked significant MVT metals. Fe-sulfide precipitation increased the relative amount of Mn incorporated into the latest dolomite zones, producing bright OM-CL and locally distinct pink dolomites. These correspondences between optical and chemical zones in carbonate cements spanning MVT mineralization highlight their potential as proxies for MVT ore mineralization and as tools for guiding exploration for zinc and other critical elements.

ACKNOWLEDGMENTS

This project was supported by the Third Mr. and Mrs. Charles E. Yager Professorship of the Jackson School of Geosciences, University of Texas at Austin (J.R. Kyle), as well as student grants from the University Research Fund, the Society of Economic Geologists, and the American Association of Petroleum Geologists (T.R. Quintero). We thank Cominco American, Inc. for cores and Nyrstar (Tennessee, USA) for mine access. We thank Jay Gregg and an anonymous reviewer for their useful critiques.

REFERENCES CITED

Anderson, G.M., 2008, The mixing hypothesis and the origin of Mississippi Valley-type ore deposits: Economic Geology, v. 103, p. 1683–1690, https://doi.org/10.2113/gsecongeo.103.8.1683.

Anderson, G.M., and Garven, G., 1987, Sulfate-sulfide-carbonate associations in Mississippi Valley-type lead-zinc deposits: Economic Geology, v. 82, p. 482–488, https://doi.org/10.2113/gsecongeo.82.2.482.

Bonnet, J., Mosser-Ruck, R., Caumon, M.-C., Rouer, O., Andre-Mayer, A.-S., Cauzid, J., and Peiffert, C., 2016, Trace element distribution (Cu, Ga, Ge, Cd, and Fe) in sphalerite from the Tennessee MVT deposits, USA, by combined EMPA, LA-ICP-MS, Raman spectroscopy, and crystallography: Canadian Mineralogist, v. 54, p. 1261–1284, https://doi.org/10.3749/canmin.1500104.

Crawford, J., and Hoagland, A.D., 1968, The Mascot–Jefferson City zinc district, Tennessee, *in* Ridge, J.D., ed., Ore Deposits of the United States, 1933–1967 (Graton-Sales Volume): New York, American Institute of Mining, Metallurgical and Petroleum Engineers, v. 1, p. 242–256.

Ebers, M.L., and Kopp, O.C., 1979, Cathodoluminescent microstratigraphy in gangue dolomite, the Mascot–Jefferson City District, Tennessee: Economic Geology, v. 74, p. 908–918, https://doi.org/10.2113/gsecongeo.74.4.908.

Fairchild, I.J., 1983, Chemical controls of cathodoluminescence of natural dolomites and calcites: New data and review: Sedimentology, v. 30, p. 579–583, https://doi.org/10.1111/j.1365-3091.1983.tb00695.x.

Gaylord, W.B., and Briskey, J.A., 1983, Geology of the Elmwood and Gordonsville mines, Central Tennessee zinc district, *in* Tennessee Zinc Deposits Field Trip Guide Book: Virginia Tech Department of Geological Sciences Guidebook 9, p. 116–151.

Gratz, J.F., and Misra, K.C., 1987, Fluid inclusion study of the Gordonsville zinc deposit, central Tennessee: Economic Geology, v. 82, p. 1790–1804, https://doi.org/10.2113/gsecongeo.82.7.1790.

Gregg, J.M., and Shelton, K.L., 2012, Mississippi Valley-type mineralization and ore deposits in the Cambrian–Ordovician great American carbonate bank, *in* Derby, J.R., et al., eds., The Great American Carbonate Bank: The Geology and Economic Resources of the Cambrian-Ordovician Sauk Megasequence of Laurentia: American Association of Petroleum Geology Memoir 98, p. 161–185, https://doi.org/10.1306/13331493M981487.

Hemming, N.G., Meyers, W.J., and Grams, J.C., 1989, Cathodoluminescence in diagenetic calcites: The roles of Fe and Mn as deduced from electron probe and spectrophotometric measurements: Journal of Sedimentary Research, v. 59, p. 404–411, https://doi.org/10.1306/212F8FA8-2B24-11D7-8648000102C1865D.

Hiatt, E.E., and Pufahl, P.K., 2014, Cathodoluminescence petrography of carbonate rocks: A review of applications for understanding diagenesis, reservoir quality, and pore system evolution, *in* Coulson, I., ed., Cathodoluminescence and Its Application to Geoscience: Mineralogical Association of Canada Short Course Series 45, p. 75–96.

Hoagland, A.D., 1976, Appalachian zinc-lead deposits: Their essential features, *in* Wolfe, K.H., ed., Handbook of Strata-Bound and Stratiform Ore Deposits: Amsterdam, Elsevier, v. 6, p. 495–534.

Kesler, S.E., Jones, H.D., Furman, F.C., Sassen, R., Anderson, W.H., and Kyle, J.R., 1994, Role of crude oil in the genesis of Mississippi Valley-type deposits: Evidence from the Cincinnati Arch: Geology, v. 22, p. 609–612, https://doi.org/10.1130/0091-7613(1994)022<0609:ROCOIT>2.3.CO;2.

Kesler, S.E., Chesley, J.T., Christensen, J.N., Hagni, R.D., Heijlen, W., Kyle, J.R., Muchez, P., Misra, K.C., and van der Voo, R., 2004, Discussion of "Tectonic controls of Mississippi Valley-type lead-zinc mineralization in orogenic forelands" by D.C. Bradley and D.L. Leach: Mineralium Deposita, v. 39, p. 512–514, https://doi.org/10.1007/s00126-004-0422-3.

Kopp, O.C., Ebers, M.L., Cobb, L.B., Crattie, T.B., Ferguson, T.L., Larsen, R.M., Potosky, R.A., and Steinberg, R.T., 1986, Application of cathodoluminescence microscopy to the study of gangue carbonates in Mississippi Valley-type deposits in Tennessee: The search for a "Tennessee trend", *in* Hagni, R.D., ed., Process Mineralogy VI: Applications to Precious Metals Deposits, Industrial Minerals, Coal, Liberation, Mineral Processing, Agglomeration, Metallurgical Products, and Refractories, with Special Emphasis on Cathodoluminescence Microscopy: Warrendale, Pennsylvania, The Metallurgical Society, p. 53–67.

Kyle, J.R., 1976, Brecciation, alteration and mineralization in the Central Tennessee zinc district: Economic Geology, v. 71, p. 892–903, https://doi.org/10.2113/gsecongeo.71.5.892.

Kyle, J.R., and Ketcham, R.A., 2015, Application of high resolution X-ray computed tomography to mineral deposit origin, evaluation, and processing: Ore Geology Reviews, v. 65, p. 821–839, https://doi.org/10.1016/j.oregeorev.2014.09.034.

Leach, D.L., Taylor, R.D., Fey, D.L., Diehl, S.F., and Saltus, R.W., 2010, A deposit model for Mississippi Valley-type lead-zinc ores: U.S. Geological Survey Scientific Investigations Report 2010-5070-A, 52 p., https://doi.org/10.3133/sir20105070A.

Lewchuk, M.T., and Symons, D.T.A., 1996, Paleomagnetism and Mississippi Valley-type ore genesis in the Ordovician Knox Supergroup of central Tennessee, *in* Sangster, D.F., ed., Carbonate-Hosted Lead-Zinc Deposits: Society of Economic Geologists Special Publication 4, p. 567–576, https://doi.org/10.5382/SP.04.43.

Machel, H.G., and Burton, E.A., 1991, Factors governing cathodoluminescence in calcite and dolomite, and their implications for studies of carbonate diagenesis, *in* Barker, C.E., and Kopp, O.C., eds., Luminescence Microscopy and Spectroscopy: Qualitative and Quantitative Applications: SEPM (Society for Sedimentary Geology) Short Course 25, p. 37–57, https://doi.org/10.2110/scn.91.25.0037.

Machel, H.G., Mason, R.A., Mariano, A.N., and Mucci, A., 1991, Causes and emission of luminescence in calcite and dolomite, *in* Barker, C.E., and Kopp, O.C., eds., Luminescence Microscopy and Spectroscopy: Qualitative and Quantitative Applications: SEPM (Society for Sedimentary Geology) Short Course 25, p. 9–25, https://doi.org/10.2110/scn.91.25.0009.

Montañez, I.P., 1996, Application of cathodoluminescent cement stratigraphy for delineating regional diagenetic and fluid migration events associated with Mississippi Valley-type mineralization in the southern Appalachians, *in* Sangster, D.F., ed., Carbonate-Hosted Lead-Zinc Deposits: Society of Economic Geologists Special Publication 4, p. 432–447, https://doi.org/10.5382/SP.04.33.

Montañez, I.P., 1997, Secondary porosity and late diagenetic cements of the upper Knox Group, central Tennessee region: A temporal and spatial history of fluid flow conduit development within the Knox regional aquifer, *in* Montañez, I.P., et al., eds., Basin-Wide Diagenetic Patterns: Integrated Petrologic, Geochemical, and Hydrologic Considerations: SEPM (Society for Sedimentary Geology) Special Publication 57, p. 101–117, https://doi.org/10.2110/pec.97.57.0101.

Montañez, I.P., and Read, J.F., 1992, Eustatic control on early dolomitization of cyclic peritidal carbonates: Evidence from the Early Ordovician Upper Knox Group, Appalachians: Geological Society of America Bulletin, v. 104, p. 872–886, https://doi.org/10.1130/0016-7606(1992)104<0872:ECOEDO>2.3.CO;2.

Potra, A., and Moyers, A., 2017, Constraints on the sources of ore metals in Mississippi Valley-type deposits in central and east Tennessee, USA, using Pb isotopes: Ore Geology Reviews, v. 81, p. 201–210, https://doi.org/10.1016/j.oregeorev.2016.09.034.

Quintero, T.R., 2020, Cementation of solution-collapse breccias in the Lower Ordovician Upper Knox Group, central Tennessee [B.S. honors thesis]: Austin, University of Texas, 119 p.

Reeder, R.J., 1991, An overview of zoning in carbonate minerals, *in* Barker, C.E., and Kopp, O.C., eds., Luminescence Microscopy and Spectroscopy: Qualitative and Quantitative Applications: SEPM (Society for Sedimentary Geology) Short Course 25, p. 77–82, https://doi.org/10.2110/scn.91.25.0077.

Richter, D.K., Götte, T., Götze, J., and Neuser, R.D., 2003, Progress in application of cathodoluminescence (CL) in sedimentary petrology: Mineralogy and Petrology, v. 79, p. 127–166, https://doi.org/10.1007/s00710-003-0237-4.

Stefani, A.B., 1995, Characterization of the spatial and temporal distribution and genetic relationship of dolomitization, secondary porosity and MVT mineralization, Upper Knox Group, central Tennessee: Implications for development of basin-wide fluid flow systems [M.S. thesis]: Riverside, University of California, 157 p.

Sylvester, P.J., and Jackson, S.E., 2016, A brief history of laser ablation inductively coupled plasma mass spectrometry (LA-ICP-MS): Elements, v. 12, p. 307–310, https://doi.org/10.2113/gselements.12.5.307.

Ukar, E., and Laubach, S.E., 2016, Syn- and post-kinematic cement textures in fractured carbonate rocks: Insights from advanced cathodoluminescence imaging: Tectonophysics, v. 690, p. 190–205, https://doi.org/10.1016/j.tecto.2016.05.001.

Printed in USA